Magnetic properties and complex magnetic phase diagram in non-centrosymmetric EuRhGe_3 and EuIrGe_3 single crystals

Arvind Maurya, P. Bonville, R. Kulkarni, A. Thamizhavel, S.K. Dhar

Journal of Magnetism and Magnetic Materials 401 (2016) 823–831

Contents lists available at ScienceDirect

Journal of Magnetism and Magnetic Materials

journal homepage: www.elsevier.com/locate/jmmm

Magnetic properties and complex magnetic phase diagram in non-centrosymmetric $EuRhGe_3$ and $EuIrGe_3$ single crystals

Arvind Maurya [a], P. Bonville [b], R. Kulkarni [a], A. Thamizhavel [a], S.K. Dhar [a,*]

[a] Department of Condensed Matter Physics and Materials Science, Tata Institute of Fundamental Research, Homi Bhabha Road, Colaba, Mumbai 400005, India

[b] CEA, Centre d'Etudes de Saclay, DSM/IRAMIS/Service de Physique de l'Etat Condensé and CNRS UMR 3680, 91191 Gif-sur-Yvette, France

ARTICLE INFO

Article history:
Received 3 March 2015
Received in revised form
8 September 2015
Accepted 29 October 2015
Available online 31 October 2015

Keywords:
$EuRhGe_3$
$EuIrGe_3$
Single crystal
Magnetic phase diagram
^{151}Eu Mössbauer spectra

ABSTRACT

We report the magnetic properties of two Eu based compounds, single crystalline $EuIrGe_3$ and $EuRhGe_3$, inferred from magnetisation, electrical transport, heat capacity and ^{151}Eu Mössbauer spectroscopy. These previously known compounds crystallise in the non-centrosymmetric, tetragonal, $I4$ mm, $BaNiSn_3$-type structure. Single crystals of $EuIrGe_3$ and $EuRhGe_3$ were grown using a high temperature solution growth method using In as flux. $EuIrGe_3$ exhibits two magnetic transition temperatures $T_{N1} = 12.4$ K, and $T_N2 = 7.3$ K, whereas $EuRhGe_3$ presents a single one at $T_N = 12$ K. ^{151}Eu Mössbauer spectra show evidence for a cascade of transitions from paramagnetic to incommensurate amplitude modulated followed by an equal moment phase at lower temperature in $EuIrGe_3$. This latter phase alone occurs in $EuRhGe_3$. In both compounds, the magnetisation measured up to 14 T suggests that the equal moment magnetic phase has a spiral spin arrangement. The field induced reorientations are also well documented in the magneto-transport data. A superzone gap is observed for the current density $J \parallel [001]$, which is enhanced by a transverse magnetic field. The magnetic phase diagram constructed from all the data is complex, revealing the presence of many phases in the $H - T$ space.

1. Introduction

The magnetic properties of several Eu-based compounds with composition $EuTX_3$, where T is a d-block transition element and X=Si or Ge, have been reported in the literature [1–6]. These compounds crystallise in the non-centrosymmetric (NCS) $BaNiSn_3$-type structure. A transition from the paramagnetic to an incommensurate, amplitude modulated state followed by a second transition to a single moment phase in $EuPtSi_3$ [1] and $EuNiGe_3$ [5] was inferred from heat capacity and ^{151}Eu Mössbauer spectroscopy. Magnetisation data on a single crystal of $EuPtSi_3$ showed the presence of anisotropy, probably of both crystalline and exchange origin. Only one magnetic transition is observed in $EuPtGe_3$ and $EuPdGe_3$ [2,3]. Further, magnetisation data on a single crystal of $EuNiGe_3$ showed that while the ab-plane is the hard plane, an unusual staircase-like behavior of magnetisation is observed along the c-axis [5]. Thus, a variety of interesting magnetic behaviours is observed in $EuTX_3$ compounds. The magnetisation in the antiferromagnetic state shows a varying degree of anisotropy which is *a priori* surprising for a spin-only (S=7/2; L=0) ion like Eu^{2+}.

The existence of iso-structural $EuIrGe_3$ and $EuRhGe_3$ is known and it was of interest to study the magnetic behaviour of these two compounds. We have probed the detailed magnetic properties of single crystalline $EuIrGe_3$ and $EuRhGe_3$ by magnetisation, resistivity and heat capacity in zero and applied fields, and ^{151}Eu Mössbauer spectroscopy. While this work was in progress, the magnetic properties of single crystalline $EuIrGe_3$ and $EuRhGe_3$ have been reported, i.e. susceptibility measurements in a field of 0.1 T, zero-field electrical resistivity and heat capacity [6]. Our main observations are in agreement with the results reported in Ref. [6]; however, our more extensive data include isothermal magnetisation at selected temperatures, susceptibility measured at a number of applied fields, magnetoresistivity, construction of magnetic phase diagram, observation of the superzone gap at the antiferromagnetic transition and ^{151}Eu Mössbauer spectra. In addition, we also prepared $LaRhGe_3$ and $LaIrGe_3$ as non-magnetic reference compounds and measured their heat capacity and electrical resistivity.

2. Experimental

Polycrystalline samples of $EuIrGe_3$ and $EuRhGe_3$ were first prepared by melting Eu (99.9% purity), Ir/Rh (99.99%) and Ge

* Corresponding author.
E-mail address: sudesh@tifr.res.in (S.K. Dhar).

http://dx.doi.org/10.1016/j.jmmm.2015.10.134
0304-8853/

(99.999%) in an arc furnace under an inert atmosphere of argon. The alloy buttons were flipped over three times and re-melted to ensure proper homogenisation. An excess of about 10% over the stoichiometric amount was taken for Eu, to compensate for the weight loss due to evaporation of Eu. Initially, we attempted to grow the single crystals of these compounds by using Sn as a solvent, as that choice had proved successful for $EuPtSi_3$ and $EuPtGe_3$, but it did not give the desired results. In a second attempt, charges of $EuIrGe_3$ and $EuRhGe_3$ and In (as solvent) were taken in the weight ratio 1:8, placed together in separate alumina crucibles and sealed in quartz ampoules under a partial pressure of 10^{-6} mbar. The sealed crucibles were placed in a box type resistive heating furnace and heated to 1100 °C at a rate of 50 °C/h. After a soaking period of 24 h, a cooling rate of 2 °C/h was employed down to 600 °C. The cooling rate was increased to 60 °C/h below 600 °C. The single crystals of $EuIrGe_3$ and $EuRhGe_3$ were separated from In-flux by centrifugation. Small traces of indium were washed away by etching the grown crystals in dilute hydrochloric acid. Polycrystalline samples of non-magnetic reference $LaIrGe_3$ and $LaRhGe_3$ were prepared by the standard technique of arc melting as described above. The magnetisation as a function of field (up to 14 T) and temperature (1.8 to 300 K) was measured using Quantum Design Magnetic properties measurement system (MPMS) and Vibration sample magnetometers (VSM). The electrical resistivity between 1.8 and 300 K and the heat capacity in zero and applied fields was measured in a Quantum Design Physical properties measurement system (PPMS) unit. ^{151}Eu Mössbauer spectra were recorded at various temperatures using a constant acceleration spectrometer with a $^{151}SmF_3$ source. Laue diffraction patterns were recorded on a Huber Laue diffractometer fitted with an image plate, while powder-diffraction spectra were recorded on a Philips PANalytical set up using Cu-Kα radiation. The crystals were cut by spark erosion electric discharge machine and oriented along the desired planes using a triple axis goniometer and Laue diffraction in the back reflection mode.

3. Results and discussion

3.1. Structure

Well faceted crystals having a platelet geometry and typical dimensions of ~5 mm × 5 mm × 1 mm were obtained after centrifuging out the In solvent. The composition of the crystals was confirmed using electron dispersive analysis by x-rays (EDAX). The powder x-ray diffraction spectra, obtained by crushing a few single crystals to powder, could be indexed to tetragonal $BaNiSn_3$-type structure.

The lattice parameters obtained by the Rietveld analysis of the powder diffraction spectra using FullProf software package [7] are listed in Table 1 and are in good agreement with the previously reported values [6,8].

3.2. Magnetisation

The inverse susceptibility, χ^{-1}, of $EuIrGe_3$, between 1.8 and 300 K, with the magnetic field (0.1 T) applied parallel to [100] and [001] directions is shown in the inset of Fig. 1. The fit of χ^{-1} to the Curie–Weiss expression $\chi(T) = \mu_{eff}^2/[8(T-\theta_p)]$ between 100 and 300 K provides the following parameters: μ_{eff}=7.94 and 7.65 μ_B, and $\theta_p = -22.1$ and -13.7 K for $H\|$ [100] and [001], respectively. The value of μ_{eff} along [100] matches exactly with the Hund's rule derived value. An antiferromagnetic interaction between the divalent Eu ions is inferred from the negative values of θ_p along the two directions. The susceptibility below 20 K is shown in the main panel of Fig. 1. There is a cusp at $T_{N1} = 12.4$ K typical of antiferromagnetic ordering, followed by a mild shoulder at 7.3 K for $H\|$ [001].

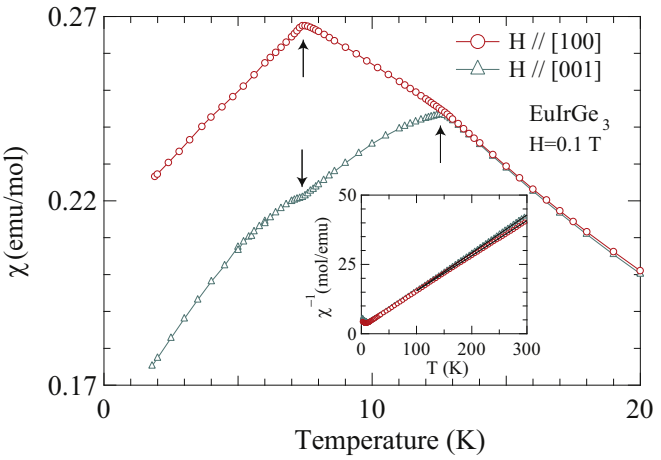

Fig. 1. Magnetic susceptibility and inverse magnetic susceptibility (in inset) of $EuIrGe_3$ at field 0.1 T along [100] and [001].

On the other hand for $H\|$ [100] there is a very subtle change of slope observed at 12.4 K and a very clear cusp is observed at 7.3 K. The main features of the susceptibility in the magnetically ordered state are in good agreement with those reported in Ref. [6]. For a collinear bipartite antiferromagnet, the susceptibility below T_N is temperature independent along the magnetic hard axis while it gradually decreases to zero along the easy axis as the temperature is lowered to zero. In the present case, χ decreases along both [001] and [100] indicating a magnetic configuration which is different from simple collinear bipartite antiferromagnetic. This is confirmed by the isothermal magnetisation data, to be described below, which suggest a spiral spin arrangement. T_{N1} is comparable to θ_p for $H\|$ [001] but it is smaller than θ_p for $H\|$ [100]. We mention here that in Ref. [6] a single θ_p value of -17 K is reported.

M(T)/H at selected fields, along [100] and [001] was measured in various fields ranging from 0.5 to 6 T and the data below 15 K are shown in Fig. 2. Additional features appear as the field is increased above 0.1 T.

At 0.5 T, *M/H* ($H\|$ [100]) shows a knee near 5.5 K, which shifts to lower temperatures as the field is increased and either vanishes at H=3 T or occurs below 1.8 K. The anomalies at 12.4 K and 7.3 K also shift slightly to lower temperatures with increasing field. For $H\|$ [001], the magnetisation between 2.5 and 4 T shows a prominent upturn at low temperatures, indicating a field-induced change in the direction of the magnetic moments. The mild shoulder at 7.3 K shifts to higher temperatures with increasing field while the peak at 12.4 K (in 0.1 T field) shifts to lower temperatures. The two appear to merge in a field of 6 T. At high fields, ~3 T and above, the magnetisation *M/H* at temperatures approaching 1.8 K is comparable for both the directions. These plots show that the configuration of the Eu moments in the magnetically ordered regime is modified by the applied field. The critical points derived from $M/H(T, H)$ have been included while constructing the $H-T$ phase diagram in Fig. 12.

The magnetisation at selected temperatures for $H\|$ [100] and

Table 1
Lattice parameters *a* and *c*, and unit cell volume *V* of $EuRhGe_3$ and $EuIrGe_3$ obtained from the Rietveld refinement of x-ray powder diffraction pattern.

Compound	*a* (Å)	*c* (Å)	*V* (Å^3)
$EuRhGe_3$	4.407(3)	10.068(7)	195.57(7)
$EuIrGe_3$	4.430(0)	10.041(6)	197.06(5)

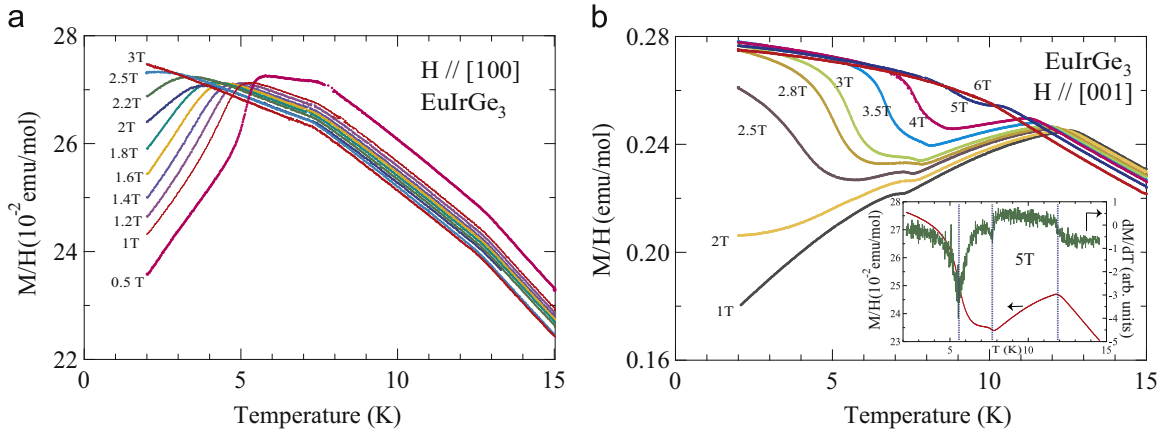

Fig. 2. Temperature dependence of M/H at selected fields along [100] (left panel) and [001] (right panel) for $EuIrGe_3$. Inset in (b) shows $M/H(T)$ at 5 T on the left scale and its derivative on the right scale with vertical dotted line at critical points.

[001] in applied fields up to 14 T is shown in Figs. 3a and b, respectively. In the inset of Fig. 3a the data at 1.8 K along the two directions are plotted. Above 3 T and between 3 and 8 T, the magnetisations at 1.8 K along the two directions virtually overlap (in conformity with the $M-T$ data discussed above) and then slightly bifurcate at higher fields. Whereas the magnetisation for $H\|$ [100] is linear with field up to about 10 T, the magnetisation along [001] shows a clear dip around 2 T at 1.8 K, which shifts to higher field as temperature increases. Such a behaviour reminds that of a planar spiral magnetic structure with sizeable anisotropy [9]: for a field perpendicular to the spiral plane, a conical structure progressively develops and the magnetisation is linear with the field; for a small field within the spiral plane, anisotropy prevents the conical structure to appear and the moments "lag" in their plane until a threshold field is reached, recovering the conical arrangement. Therefore, the susceptibility in this latter case is lower than for the perpendicular case, yielding both the observed dip in the $M(H)$ curve and the lower M/H values reported above. For $EuIrGe_3$, this suggests that the plane of the spiral is perpendicular to [100] and contains [001].

At 1.8 K, the magnetisation at 14 T along [001] (6.3 μ_B/Eu) is slightly larger than along [100] (6.15 μ_B/Eu), and the saturation value of 7 μ_B is not reached along both directions. Thus the spin-flip field at 1.8 K is nearly independent of the direction (like in $EuPtGe_3$) and should be close to 16 T.

In contrast to $EuIrGe_3$, the Rh analog shows only one antiferromagnetic transition which occurs close to $T_N = 12$ K in applied field of 0.1 T (see, Fig. 4), in accordance with Ref. [6]. Fig. 4 shows the susceptibility data below 20 K for $H\|$ [100], [110] and [001]. It is noticed that the response in the *ab*-plane is isotropic. Above 100 K, the inverse susceptibility fits well to the Curie–Weiss law with the values: μ_{eff}=7.56 and 7.78 μ_B, $\theta_p = -7$ and -11 K for $H\|$ [100] and [001], respectively. It is likely that the value of μ_{eff} is slightly lower due to the presence of tiny inclusions of In metal in the crystal which get incorporated during the crystal growth. As a result the amount of Eu used in the calculation of μ_{eff} is actually slightly overestimated. We infer the presence of In from the slight drop in the susceptibility measured in an applied field of 0.005 T near the superconducting transition temperature of In. The drop vanishes when the applied field is increased to 0.05 T.

At higher fields applied parallel to [100] the transition shifts to lower temperatures reaching 9.4 K in 10 T (see, Fig. 5a). An additional peak which occurs close to 11 K in 1 T gradually shifts to 2.8 K in 8 T. Between 4 and 6 T, the magnetisation shows additional features below 5 K which are depicted in Fig. 5b. The field induced changes in the magnetic configuration have a first order character as indicated by the hysteresis observed at 5 T (see inset of Fig. 5a). The data depicted in Figs. 5a and 5b indicate a field induced complex phase diagram. On the other hand, for fields along the [001] direction the character of the plots remains unaltered except that T_N decreases with field (see Fig. 5c). While our observations do not provide us the actual configuration of the magnetic moments, they appear to suggest a non-collinear antiferromagnetic structure which evolves in a complex fashion for field applied in the *ab*-plane.

The main panel of Fig. 6a shows the isothermal magnetisation plots at 2 K for $H\|$ [100], [110] and [001]. The magnetisation along [100] at various temperatures is plotted in Fig. 6b; the inset shows the magnetisation at 2 and 5 K for $H\|$ [001].

Along [001] the magnetisation increases nearly linearly with the field reaching a value of 6.2 μ_B/Eu ion at 14 T. There is hardly any change in the magnetisation at 2 and 5 K (Fig. 6b inset). By contrast, for $H\|$ [100] and [110], one sees a deviation from linearity as a large dip up to 5 T. This behaviour could be due to a spiral spin arrangement, like in $EuIrGe_3$, but with the plane of the spiral perpendicular to [001]. Furthermore, the structure observed in the dip near 3.5 T could point to a still more complex moment arrangement. Above 10 T, the *ab*-plane isotropy of the magnetisation is slightly violated. At the highest field (14 T) the magnetisations along the three directions are nearly identical. A derivative plot of magnetisation for $H\|$ [100], dM/dH, shown in the inset of Fig. 6a shows three peaks which are a signature of the field induced changes in the magnetic configuration. The magnetisation shows hysteresis around 5 T at 2 K (see, upper inset of Fig. 6a) which correlates nicely with the data depicted in the inset of Fig. 5a. The temperature dependence of $M(H)$ along [100] is shown in main panel of Fig. 6b.

3.3. Heat capacity

The specific heat measured down to 100 mK in zero field (Fig. 7a) confirms the presence of two transitions in $EuIrGe_3$, at $T_{N1} = 12.4$ and $T_{N2} = 7.2$ K, in close correspondence with the low-field magnetisation data presented above. The magnitude of the jump in the heat capacity at T_{N1}, ~5 J/mol K, which is far below the mean-field value of 20.14 J/mol K for a mol of spin $S=7/2$. This suggests that the transition at T_{N1} is from paramagnetic to amplitude modulated antiferromagnetic configuration. At T_{N2} the transition from this intermediate state to an equal moment configuration takes place, as confirmed by ^{151}Eu Mössbauer spectra (see below).

The heat capacity was also measured in applied fields of 8 and 14 T with $H\|$ [100]. At 8 T, the two peaks at 7.2 and 12.4 K (zero field) have shifted slightly lower in temperature to 6.1 and 11 K,

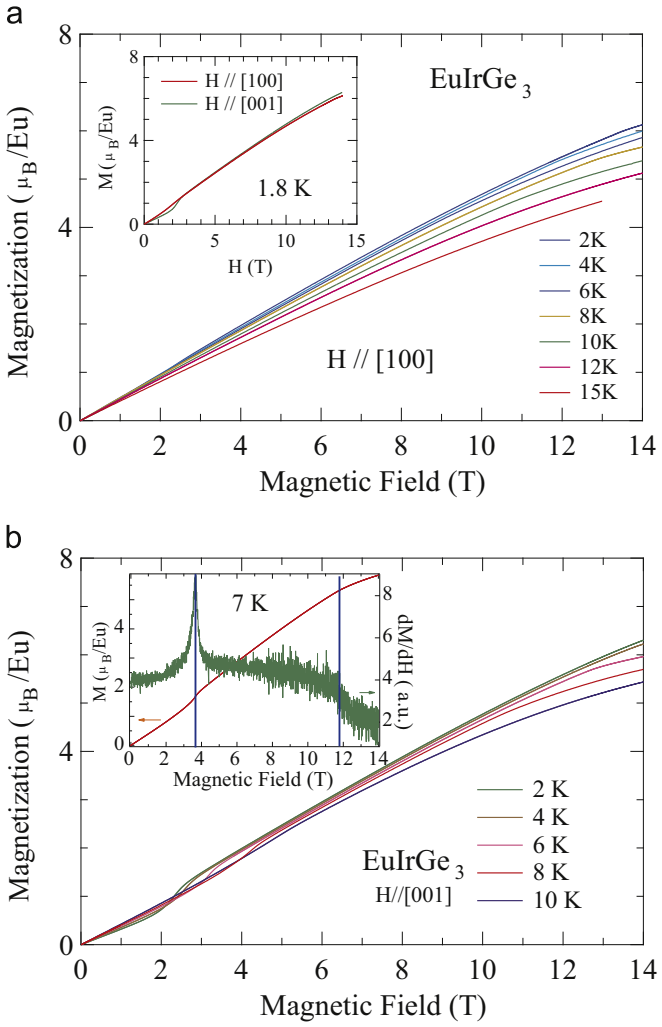

Fig. 3. Field dependence of magnetisation at selected temperatures in $EuIrGe_3$ along (a) [100] and (b) [001]. Inset in (a) represents nearly isotropic magnetisation plots in $EuIrGe_3$ and in (b) a representative derivative of magnetisation plot along [001] at 7 K (right scale) along with the $M(H)$ data (left scale) is shown. (For interpretation of the references to color in this figure caption, the reader is referred to the web version of this paper.)

respectively, in correspondence with the magnetisation data shown in Fig. 2. The jump in the heat capacity is slightly reduced. At 14 T, there is only one peak at 7 K, with appreciable reduction in peak height. For $H\|$ [001], at 5 T both peaks come closer but are still well resolved; at higher fields we observe only a single peak in agreement with magnetic phase diagram in Fig. 12b.

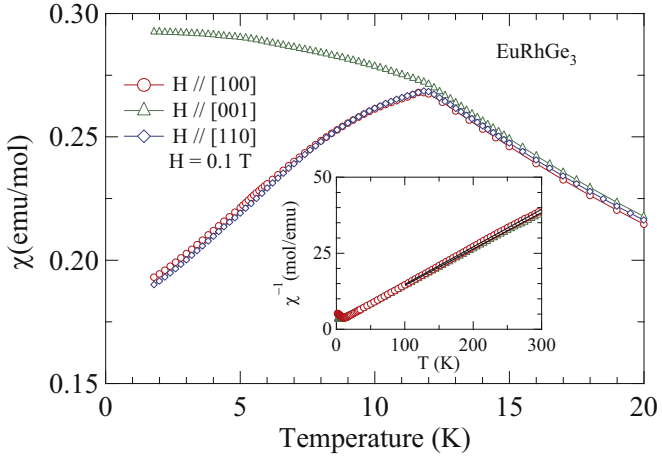

Fig. 4. Anisotropic magnetic susceptibility and inverse magnetic susceptibility (in inset) as a function of temperature at magnetic field 0.1 T of $EuRhGe_3$.

The heat capacity of the iso-structural $LaIrGe_3$ is also plotted in Fig. 7a, and the 4*f* contribution to the heat capacity, C_{4f}, and entropy S_{4f} were calculated under the assumption that the phonon heat capacities of $LaIrGe_3$ and $EuIrGe_3$ are identical, after normalisation due to the slightly different atomic masses of La and Eu. The entropy attains the value of $R \ln 8$ (for Eu^{2+} ions, $S=7/2$ and $L=0$) near 18 K but keeps on increasing at higher temperatures, indicating a poor validity of the assumption of identical phonon spectra in $LaIrGe_3$ and $EuIrGe_3$ at least at higher temperatures. A similar situation was earlier encountered in $EuPtSi_3$ [1]. The C/T vs. T^2 plot of $LaIrGe_3$ is linear below 8 K, characterized by $\gamma = 4.0$ mJ/mol K^2 and $\beta = 0.349$ mJ/mol K^4. A Debye temperature, θ_D, of 303 K is inferred from β.

The heat capacity data of $EuRhGe_3$ measured in zero and 8 T ($H\|$ [100]) are plotted in Fig. 7b. The relatively sharp jump in the heat capacity near 12 K in zero field is in excellent agreement with the magnetisation data discussed above. Surprisingly, the jump in the heat capacity at T_N in $EuRhGe_3$ is about 13 J/mol K, which is far below the value for a transition to an equal moment antiferromagnetic state (20.14 J/mol K) in the mean field model [10]. It may be noted that the shape of the heat capacity variation below T_N is rather unusual and similar to some cases of amplitude modulated moment state described in Fig. 5 in Ref. [10]. In applied fields the magnetic transition shifts to lower temperatures and additional peaks, marked by downward arrows in Fig. 7 for 5 T data are observed, in conformity with the in-field magnetisation data (Fig. 5) described above. The heat capacity of non-magnetic, reference analogue $LaRhGe_3$ is also plotted. The entropy S_{4f} was estimated using the method mentioned above. It again exceeds the maximum value of $R \ln 8$ like in the Ir compound. For $LaRhGe_3$, $\gamma = 6.7$ mJ/mol K^2 and $\beta = 0.376$ mJ/mol K^4. A Debye temperature, θ_D, of 296 K is inferred from β, which is close to that of the Ir compound.

3.4. Electrical resistivity

The electrical resistivity of $EuIrGe_3$ and $EuRhGe_3$ with the current density J parallel to [100] and [001], respectively, is shown in Fig. 8. The resistivity shows anomalies for $EuIrGe_3$ at the two transitions T_{N1} and T_{N2} along both directions though with slightly different characteristics. Along [100] the resistivity decreases faster at each transition due to the rapid reduction in the spin-disorder scattering. Above T_{N1} the resistivity monotonically increases up to the room temperature. On the other hand, for $J\|$ [001] at T_{N1} there is a slight upturn on cooling. The upturn at T_{N1} is suggestive of a gap-opening at the Fermi surface along [001] direction with AFM order, often referred to as superzone gap. Many other rare earth intermetallics have been found to show this kind of behaviour [11–13].

The electrical resistivity of $EuRhGe_3$ has some similarities with that of $EuIrGe_3$ described above. For $J\|$ [100] the resistivity decreases at the single antiferromagnetic transition, while for $J\|$ [001] the initial increase at T_N (=12 K) again indicates the opening of a superzone gap like in $EuIrGe_3$.

We have fitted the Bloch Grüneisen expression to our $\rho(T)$ data in the paramagnetic region given by following expression:

$$\rho(T) = A + B\left(\frac{T}{\theta_R}\right)^5 \int_0^{\theta_R/T} \frac{x^5}{(e^x - 1)(1 - e^{-x})} dx \quad (1)$$

where θ_R is the Debye temperature determined from the $\rho(T)$ data, A is the temperature independent part of resistivity comprising of electron scattering caused by crystal imperfections and spin

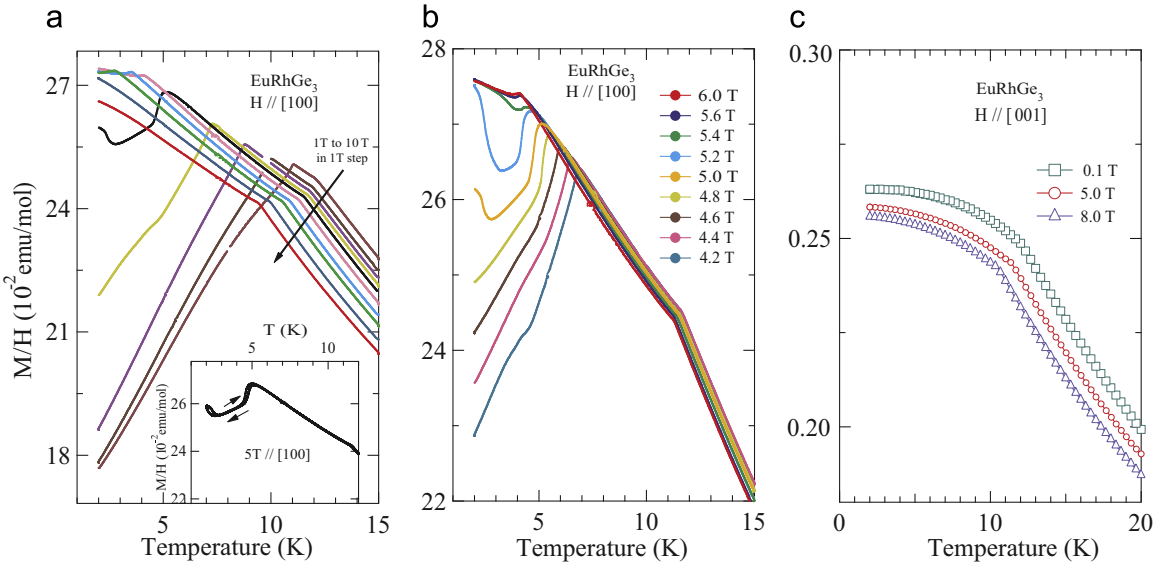

Fig. 5. $M(T)/H$ at selected fields along [100] (a and b) and [001] (c) for $EuRhGe_3$. Inset in (a) shows the hysteresis in the data taken in the warming and cooling cycle at 5 T.

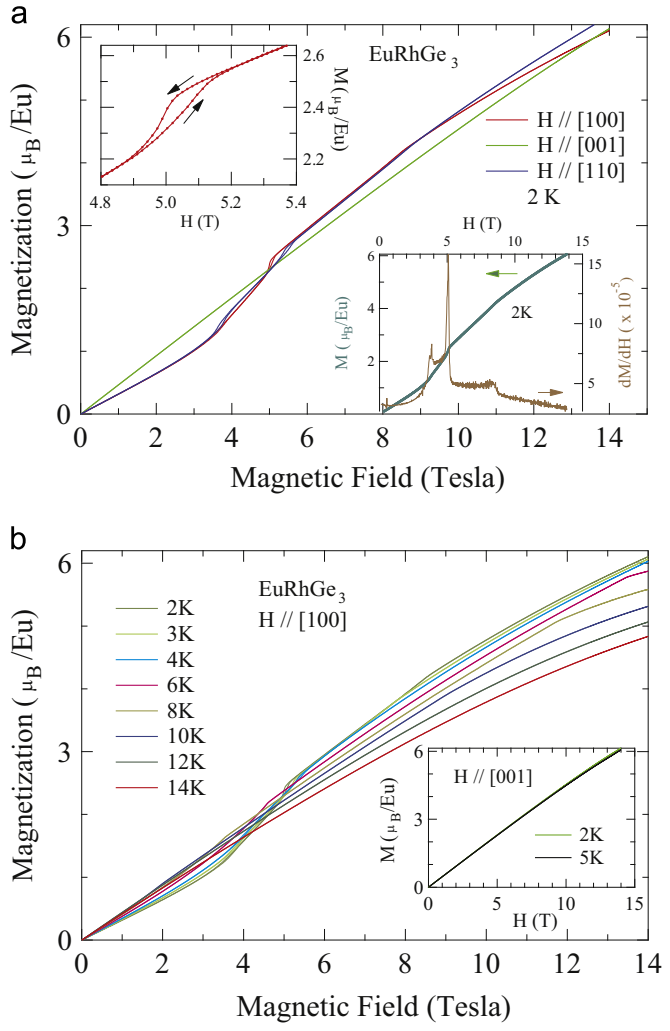

Fig. 6. (a) Isothermal magnetisation $M(H)$ at 2 K of $EuRhGe_3$ along the principal crystallographic directions. Bottom inset shows $M(H)$ at 2 K on left scale and its derivative on right scale revealing field induced spin reorientations. (b) Temperature evolution of $M(H)$ of $EuRhGe_3$ along [100] in main panel and along [001] in the inset. (For interpretation of the references to color in this figure caption, the reader is referred to the web version of this paper.)

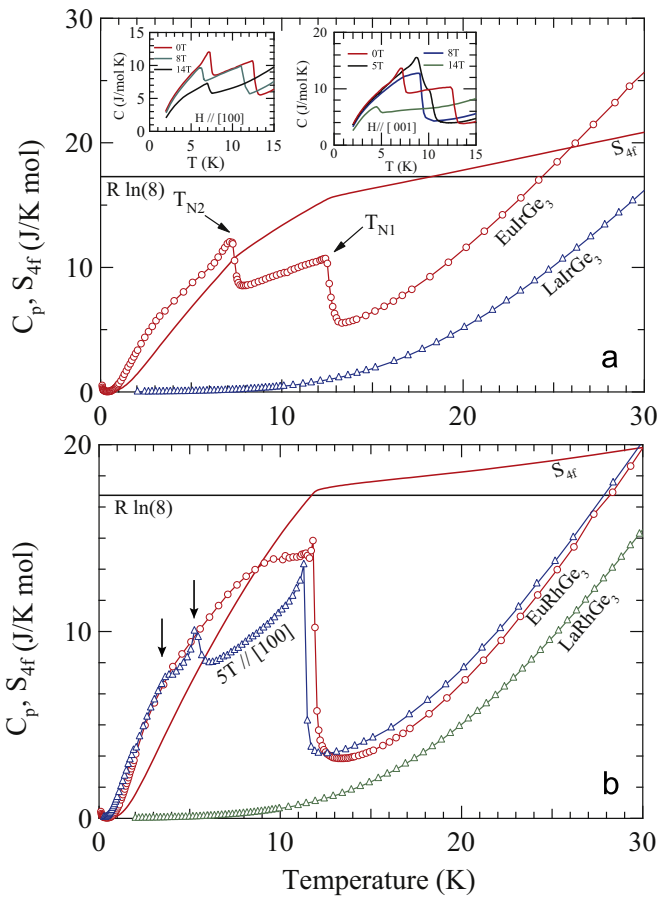

Fig. 7. Heat capacity ($C_p(T)$) and calculated magnetic entropy (S_{4f}) of (a) $EuIrGe_3$ and (b) $EuRhGe_3$, respectively. $C_p(T)$ of corresponding La-analogues are also shown in the main panels. Insets in (a) show the $C_p(T)$ curves when field is applied along [100] (left) and [001] (right). In (b), blue trace represents data taken at 5 T field applied parallel to a-axis, capturing the field induced phase transitions indicated by arrows. (For interpretation of the references to color in this figure caption, the reader is referred to the web version of this paper.)

disorder in the paramagnetic state and B is a material dependent prefactor. Parameters determined from the fit are listed in Table 2. It may be noted that the magnitude of θ_R is different from θ_D. This

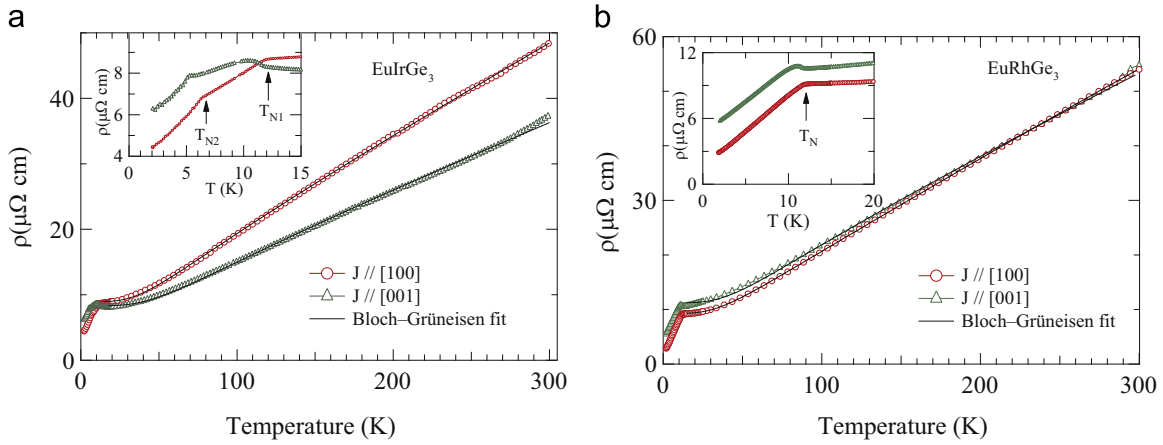

Fig. 8. Variation of electrical resistivity ($\rho(T)$) for current density $J\|$ [100] and [001] for (a) $EuIrGe_3$ and (b) $EuRhGe_3$. Insets show low temperature data on an expanded scale where the magnetic transitions are marked by arrows.

is not unusual as θ_R considers only the longitudinal lattice vibrations.

The transverse magnetic field dependence of electrical resistivity under different configurations is shown in Figs. 9 and 10 for $EuIrGe_3$ and $EuRhGe_3$, respectively. The main features in the $\rho(T)$ data of both compounds are in excellent correspondence with the magnetic susceptibility data. The upturn in the resistivity at T_N becomes more prominent as the field is increased (see, Figs. 9a and 10a), suggesting an enhancement of the superzone gap in the two compounds.

The magnetoresistivity *MR*, defined as $MR(H) = (\rho(H) - \rho(H=0)) \times 100/\rho(H=0)$, of $EuIrGe_3$ for different transverse configurations is shown in Figs. 11(a–c). For $H\|$ [001], [010] and $J\|$ [100] at $T=2$ K, the *MR* is positive, increases rapidly with field and shows a minor anomaly near 2 T which corresponds well with the spin-flop like transition seen in the magnetisation. The positive *MR* is typically expected in an antiferromagnet as the field disrupts the antiferromagnetic ordered state. The positive *MR* peaks near 12 T and then decreases slightly, indicating the proximity of the spin-flip field around 14 T. As the temperature is raised (see, Fig. 10c) the minor anomaly shifts to higher fields tracking the corresponding increase of the spin-flop like transition field in the magnetisation, and the magnitude of positive *MR* decreases due to the increase of temperature. At 6 K the *MR* becomes negative for $H > 10$ T, and the crossover field value decreases with further increase of temperature. At 15 K the *MR* in the paramagnetic state is negative at all fields, most likely due to the ordering effect of the field on the fluctuating moments.

The *MR* for $H\|$ [010] shows qualitatively similar field dependence (see, Fig. 10b) as described above for $H\|$ [001]. The anomalies observed in *MR* data are included in phase diagram corresponding well to the magnetisation data.

The *MR* of $EuRhGe_3$ at selected temperatures is shown in Figs. 11(d–f). Fig. 11d shows a comparison between *MR* data taken at 2 K in different configurations. The nature of *MR* curves is dependent upon the field direction as well as the direction of current density *J*. For $H\|$ [100] and $J\|$ [001] the *MR* at 2 K is positive and initially increases with field. It shows anomalies at 5 and 8.5 T which mirror the anomalies seen in the magnetisation at these fields (Fig. 5b). Above 8.5 T, the *MR* is still positive but begins to decline in its absolute values most likely due to the increasing alignment of the moments along the field direction as the spin-flip field is approached. As the temperature is increased, the two anomalies approach each other, shifting in opposite directions, and above ~4–5 K they apparently merge and then the single anomaly shifts to lower fields with increasing temperature (see Fig. 11e). At 6 K, the *MR* shows an anomaly in 13–14 T range which shifts to 11–12 and 8–9 T intervals at 8 and 10 K, respectively. This feature matches well with the magnetisation plots measured at these temperatures (indicated by arrows in Fig. 6b). In the paramagnetic region (15 and 20 K) the *MR* is negative. Lastly, the *MR* data for $H\|$ [001] and $J\|$ [100] are shown in Fig. 11f. It may be recalled that [001] is relatively the hard-axis of magnetisation in $EuRhGe_3$. The *MR* up to 5 K is positive, increasing with field and showing a slight decline above 12 T. At 8 and 10 K the decline in *MR* is marked by a sharp knee at ~11.5 and ~9 T, respectively, which are phenomenologically similar to the one's seen in Fig. 11e and occur at similar values of fields as well, and may have a similar origin. Again, the *MR* in the paramagnetic region is negative.

Table 2
Parameters derived from the Bloch Grüneisen fit to the $\rho(T)$ data of $EuRhGe_3$ and $EuIrGe_3$.

	$EuRhGe_3$		$EuIrGe_3$	
	$A(\mu\Omega\text{cm})$	$\theta_R(K)$	$A(\mu\Omega\text{cm})$	$\theta_R(K)$
$J\|$ [100]	9.5	246	8.9	224
$J\|$ [001]	11.2	244	8.3	270

3.5. Magnetic phase diagram

From $M(T, H)$ and $\rho(T, H)$ data we have constructed the magnetic phase diagrams of $EuRhGe_3$ and $EuIrGe_3$ shown in Fig. 12. The conclusions derived from these two sets of data correspond very well with each other. AF1, AF2,… denote phases specified by different antiferromagnetic (or spiral/conical) configurations. In $EuRhGe_3$, at low fields a second transition appears which shifts to lower temperatures with increasing magnetic field until the occurrence of a tricritical point at (5 K, 4.9 T), followed by another tricritical point at (4 K, 5.4 T). Dotted lines are plausible extrapolations.

The magnetic phase diagram in $EuIrGe_3$ also shows a similar degree of complexity. Here the red symbols have been used for points determined from $H\|$ [001] and blue symbols for $H\|$ [100] data, respectively for the *M* vs. *T*, *M* vs. *H*, *R* vs. *H* and *R* vs. *T* experiments. For $H\|$ [001], on increasing the field, T_{N1} and T_{N2} come closer and merge together accompanied with the appearance of other field induced transitions forming a closed dome centered around 10 K. This dome corresponds to the incommensurate modulated phase. Above 5 T we could observe only one transition along the *c*-axis. On the other hand, for field parallel to the *a*-axis

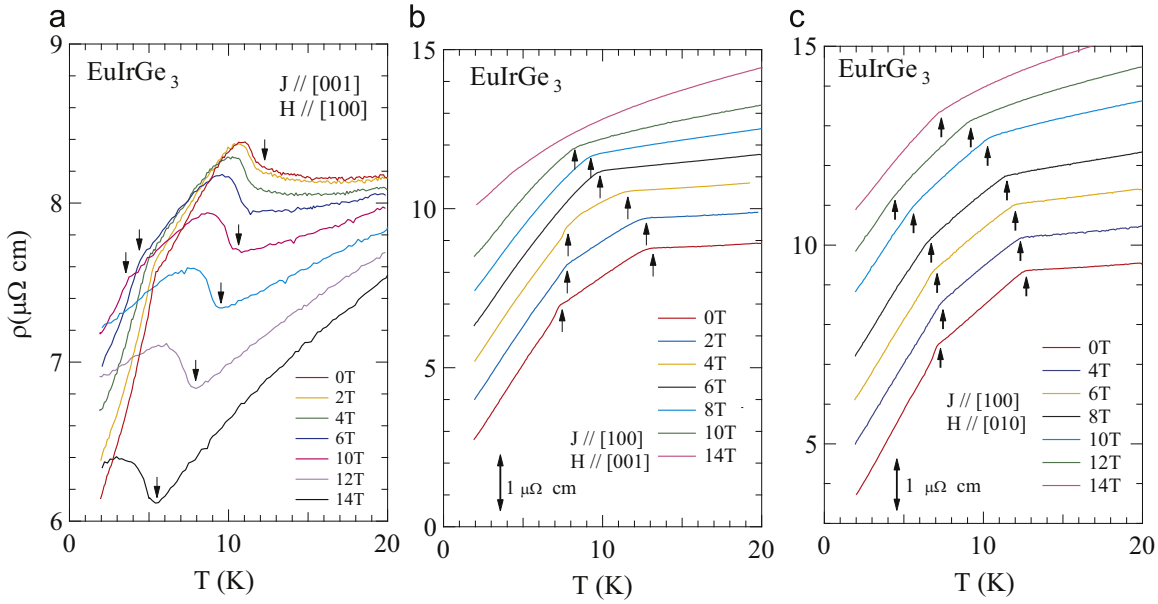

Fig. 9. $\rho(T)$ of $EuIrGe_3$ for different configurations of current and applied magnetic fields. In b and c, the traces for non-zero fields have been moved in vertical direction for clarity. Arrows indicate magnetic phase transitions. (For interpretation of the references to color in this figure caption, the reader is referred to the web version of this paper.)

T_{N1} and T_{N2} are suppressed, apparently merging at around 14.2 T at absolute zero. Interestingly, it looks that the high field phase for $H\|$ [001] seems to converge at the same point at 0 K as the merging point of two phase lines for $H\|$ [100]. An additional low field phase line nearly parallel to the temperature axis, having opposite curvatures for *a* and *c* axes but merging with each other at around 2 K is observed. It may be noted that the phase boundary between PM and AF1 phase is also a demarcation line for the superzone gap in both $EuRhGe_3$ and $EuIrGe_3$.

3.6. ^{151}Eu Mössbauer spectra

The ^{151}Eu Mössbauer spectra at 4.2, 8 and 12 K in $EuIrGe_3$ are shown in Fig. 13. The 4.2 K spectrum is a hyperfine field pattern with the single value H_{hf}=28.9(2) T, and it shows an isomer shift of −10.6(1) mm/s with respect to the SmF_3 γ-ray source. Both these values are characteristic of divalent Eu, and the single hyperfine field indicates an equal moment magnetic ordering. At 8 K, just above T_{N2}, the spectrum has changed shape and cannot be fitted using a single hyperfine field. Its shape is typical of an incommensurate magnetic structure (see for instance Ref. [5]), and it was fitted to a lineshape where the hyperfine field distribution is decomposed into its Fourier components:

$$H_{hf}(kx) = \sum_n m_{2n+1} \sin[(2n+1)kx], \tag{2}$$

where n is an integer running from zero to a maximum value n_{max}, and kx runs from 0 to 2π, x being the distance along the propagation vector **k**. A good fit was obtained with n_{max}=4, i.e. with 5 Fourier components, yielding a modulation with a maximum hyperfine field value of 29 T, equal to the 4.2 K single value. At 12 K, just below T_{N1}, the spectrum is broad and featureless, and can be fitted to a superposition of an incommensurate pattern, with maximum hyperfine field 17 T, and of a single narrow line characteristic of the paramagnetic phase, as observed at 15 K (spectrum not shown). The coexistence of the two phases close to T_{N1}

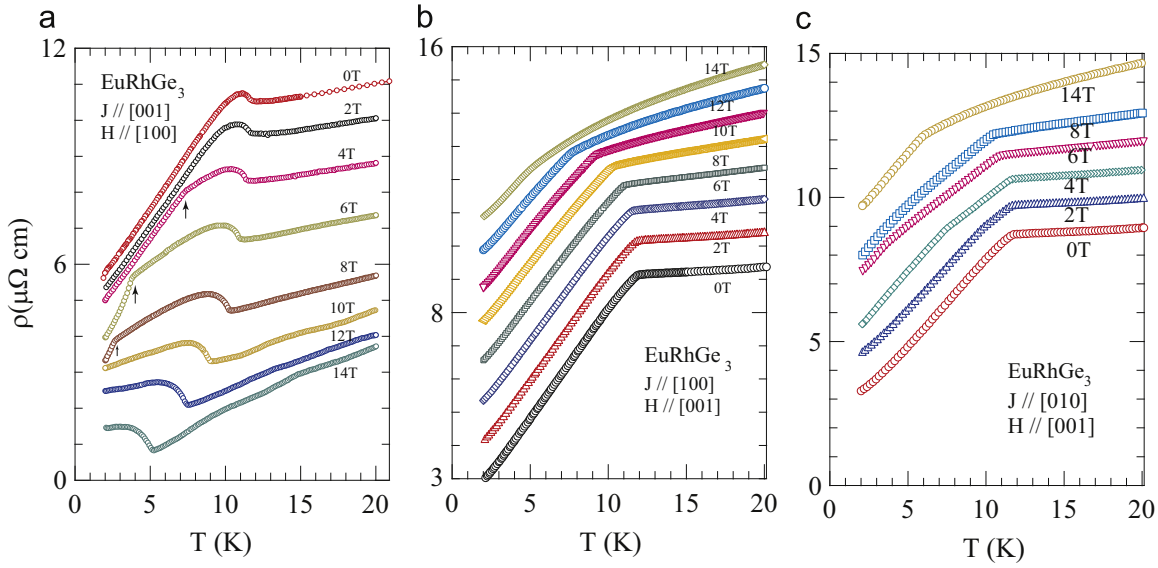

Fig. 10. $\rho(T)$ of $EuRhGe_3$ for different configurations of current and applied magnetic fields. $\rho(T)$ curves other than 0 T have been shifted vertically for clarity.

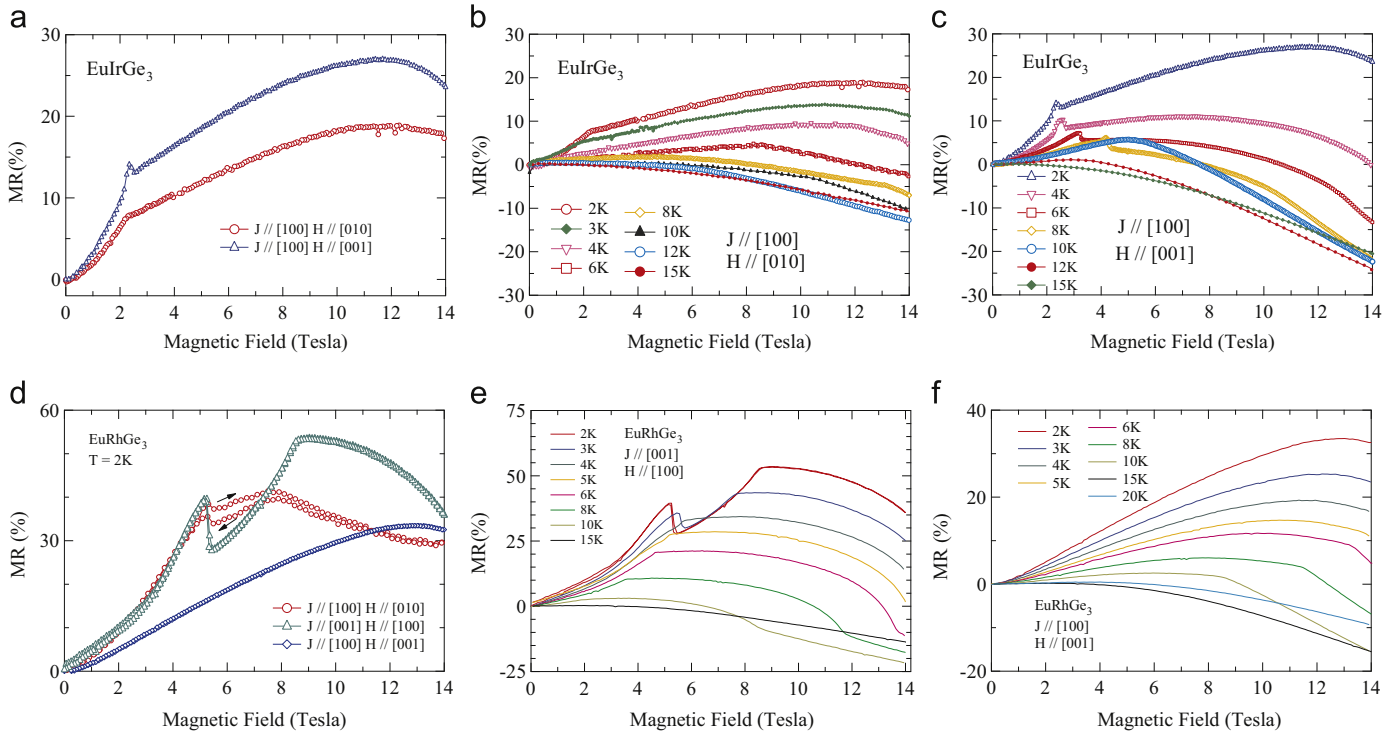

Fig. 11. The variation of magnetoresistance with field at selected temperatures in $EuIrGe_3$ (upper panels) and $EuRhGe_3$ (lower panels).

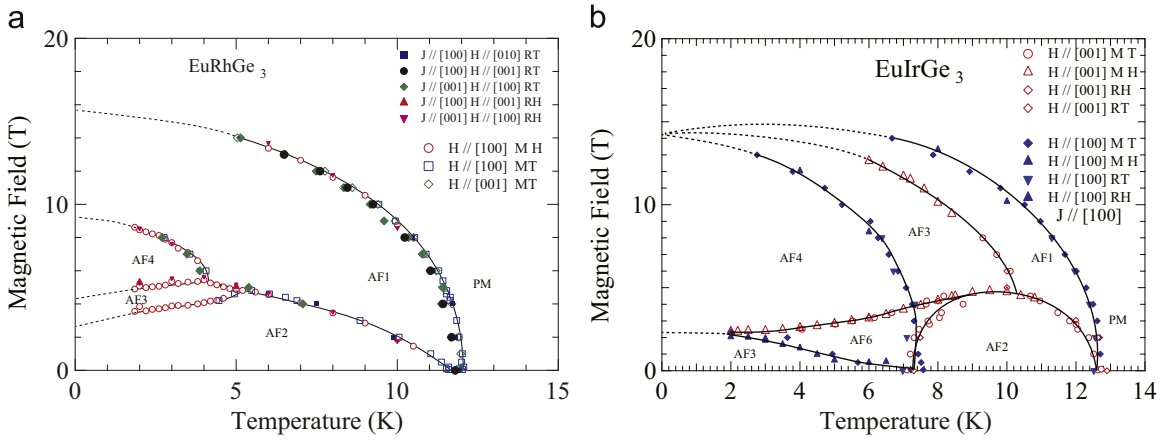

Fig. 12. $H-T$ phase diagram of (a) $EuRhGe_3$ and (b) $EuIrGe_3$ constructed from critical points in $M(T, H)$ and $\rho(T, H)$ data. Solid lines are guide to the eye and dotted lines are extrapolation.

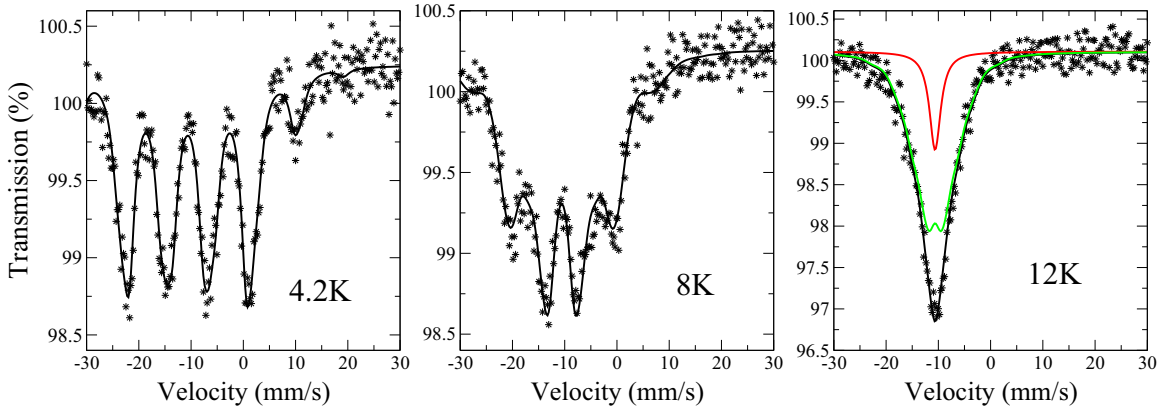

Fig. 13. ^{151}Eu Mössbauer spectra at selected temperatures in $EuIrGe_3$, in the equal moment phase (4.2 K), close to the equal moment incommensurate transition (8 K) and close to the incommensurate-paramagnetic transition (12 K). At 12 K, the green subspectrum represents the incommensurate pattern and the red subspectrum the paramagnetic pattern. (For interpretation of the references to color in this figure caption, the reader is referred to the web version of this paper.)

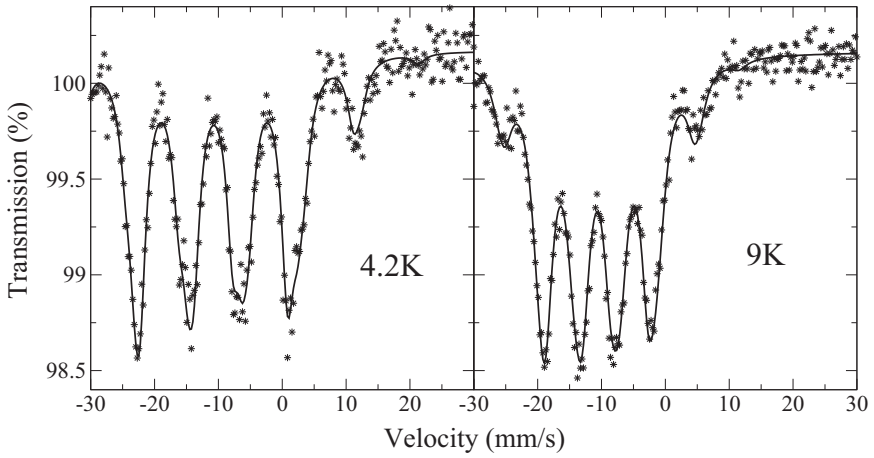

Fig. 14. ^{151}Eu Mössbauer spectra in $EuRhGe_3$at 4.2 K and 9 K fitted to a single hyperfine field pattern.

points to a probable first order character of the paramagnetic to incommensurate magnetic phase transition. For $EuRhGe_3$, the Mössbauer spectra recorded at 4.2 and 9 K, shown in Fig. 14, are single hyperfine field patterns, with values respectively 29.8 T and 20.7 T. So, in agreement with the previous thermodynamic measurements, $EuRhGe_3$ presents a single magnetic transition.

Of the five compounds $EuPtSi_3$, $EuNiGe_3$, $EuIrGe_3$, $EuPtGe_3$ and $EuRhGe_3$ in which the ^{151}Eu Mössbauer data have been taken, the first three show a cascade of magnetic transitions, the intermediate phase being amplitude modulated. In $EuPtGe_3$, where the magnetisation is rather isotropic, no intermediate phase is present and it was conjectured that multiple transitions may be linked to anisotropy [5]. The isothermal magnetisation of $EuIrGe_3$ is rather similar to that of $EuPtGe_3$, yet it shows a cascade of transitions. This shows that other factors are important.

Neutron diffraction studies, now relatively feasible in Eu materials, are clearly required to determine the moment configurations in these compounds. We note that, in addition to the two present germanides, the Pt based $EuPtSi_3$ and $EuPtGe_3$ materials should show a spiral magnetic structure in their equal moment phase, as witnessed by the dips in their magnetisation curves, which had not been interpreted in our previous publications [1,2].

References

[1] N. Kumar, S.K. Dhar, A. Thamizhavel, P. Bonville, P. Manfrinetti, Phys. Rev. B 81 (2010) 144414.
[2] N. Kumar, P.K. Das, R. Kulkarni, A. Thamizhavel, S.K. Dhar, P. Bonville, J. Phys.: Condens. Matter 24 (2012) 036005.
[3] D. Kaczorowski, B. Belan, R. Gladyshevskii, Solid State Commun. 152 (2012) 839.
[4] R.J. Goetsch, V.K. Anand, D.C. Johnston, Phys. Rev. B 87 (2012) 064406.
[5] A. Maurya, P. Bonville, A. Thamizhavel, S.K. Dhar, J. Phys.: Condens. Matter 26 (2014) 216001.
[6] Oleksandr Bednarchuk, Anna Gagor, Darius Kaczorowski, J. Alloys Compd. 622 (2015) 432.
[7] Juan Rodriguez-Carvajal, Physica B 192 (1993) 55.
[8] G. Venturini, M. Méot-Meyer, B. Malaman, B. Roques, J. Less-Common Met. 113 (1985) 197.
[9] A. Herpin, in: Théorie du magnétisme, Presses Universitaires de France, Paris, 1968.
[10] J.A. Blanco, D. Gignoux, D. Schmitt, Phys. Rev. B 43 (1991) 13145.
[11] N. Kumar, P.K. Das, N. Kumar, R. Kulkarni, S.K. Dhar, A. Thamizhavel, J. Phys.: Condens. Matter 24 (2012) 146003.
[12] V.K. Anand, D.C. Jhonston, J. Phys.: Condens. Matter 26 (2012) 286002.
[13] Z. Hossain, C. Geibel, N. Senthilkumaran, M. Deppe, M. Baenitz, F. Schiller, S. L. Molodtsov, Phys. Rev. B 69 (2004) 014422.